2009 American Control Conference
Hyatt Regency Riverfront, St. Louis, MO, USA
June 10-12, 2009

Control-based Approach to Broadband Viscoelastic Spectroscopy: PDMS example†

Zhonghua Xu, Qingze Zou, Pranav Shrotriya and Ping Xie ‡

Abstract— **In this article, a novel nanoscale broadband viscoelastic spectroscopy approach is proposed. The proposed approach utilizes the recently developed model-less inversion-based iterative control (MIIC) technique for accurate measurement of the material response to the applied excitation force over a broad frequency band. Current nanomechanical measurement is slow and narrow-banded and thus not capable of measuring rate-dependent phenomena of materials. In the proposed approach, an input force signal with dynamic characteristics of band-limited white-noise is utilized to rapidly excite the nanomechanical response of the material over a broad frequency range. Then, the MIIC technique is used to compensate for the hardware adverse effects, thereby allowing the precise applications of such an excitation force and measurement of the material response (to the applied force). The proposed approach is illustrated by implementing it to measure the creep compliance of poly(dimethylsiloxane) (PDMS) over a broad frequency range over 3 orders of magnitude.**

I. INTRODUCTION

In this article, a novel nanoscale broadband viscoelastic spectroscopy (NBVS) methodology is proposed. The proposed NBVS approach utilizes the recently developed model-less inversion-based iterative control (MIIC) technique [1] to allow rapid excitation and subsequent measurement of the nanomechanical behavior of materials over a broad frequency band. The scanning probe microscope (SPM) has become an enabling tool to quantitatively measure the mechanical properties of a wide variety of materials [2]. Current SPM-based force measurements, however, are limited by the slow operation of SPM to measure the rate-dependent phenomena of materials [3], and large measurement (temporal) errors can be generated when dynamic evolution of the material is involved during the measurement. Operating speed of current SPMs is limited by: (1) the excitation force applied, which is either quasi-static or resonant-oscillation based, is either too narrow-banded in frequency (quasi-static) or too slow (resonant oscillation based) to rapidly excite the nanomechanical behavior of materials over a broad frequency band; and (2) the hardware adverse effects can be coupled into the measured data if the measurement is at high-speed and over a broad frequency range. These adverse effects include the hysteresis of the piezo actuator (used to position the probe relative to the sample), the vibrational dynamics of the piezo actuator and the probe along with the mechanical parts, and the dynamics uncertainties.

† The work is support by NSF Grants CMMI-0626417 and DUE-0632908, which are gratefully acknowledged.

‡ Z. Xu, Q. Zou and P. Shrotriya are with Mechanical Engineering, Iowa State University, Ames, IA, USA 50011. P. Xie is a visiting scholar from the Yanshan University, China. Q. Zou is the corresponding author (qzzou@iastate.edu).

In usual force-curve measurements, the applied input force follows a triangle trajectory [2]. Such an excitation input is quasi-static and does not contain rich frequency components required to rapidly excite broadband viscoelastic response of materials. One attempt at addressing the lack of frequency components in input force has been through the development of force modulation technique [4], where a sinusoidal force signal (i.e., ac signal) of small amplitude is superposed on the triangle input force and applied during the measurement. During the measurement, the hardware dynamic response is coupled into the measured data and must be accounted-for afterwards using a dynamics model [4]. As a result, the load/unload rate are limited to small range because the oscillation amplitude ($<$100 nm) and the oscillation frequency (a few hundred Hz) have to be kept small [4] such that dynamics coupling can be adequately captured by using a simple spring-mass-damper model. Moreover, force-modulation technique is slow for measuring material response over a large frequency range, because the de-modulation process must be applied to accurately measure the amplitude and the phase shift of the oscillation, which is inherently time-consuming. During high-speed force measurements, the SPM dynamics consisting of the piezo actuator and the probe [5] can be excited, resulting in large vibrations of the probe relative to the sample, which in turn, leads to large errors in the obtained force measurements. Furthermore, substantial dynamics uncertainties exist in the SPM system due to the change of operation condition (e.g., change of the probe), which makes the compensation of such dynamics effect challenging. When the displacement of the piezo actuator is large during the force measurement, the hysteresis effect of the piezo actuator becomes pronounced, further exacerbating large measurement errors. Therefore, a measurement technique that can accurately decouple the hardware dynamics, nonlinear hysteresis, dynamic uncertainties from the high speed force measurements is required for accurate material characterization.

The main contribution of this article is the development of an iterative control-based NBVS methodology that utilizes: system identification based approach for characterizing broadband response of materials; and advanced control techniques for deconvoluting the hardware induced errors from the measured data. First, we view the nanomechanical response of materials as a dynamic system, which thereby can be measured by exciting the system (i.e., the material) with an input force with rich frequency components, and measuring the resulting response of the material. Particularly, we employ a band-limited white-noise type of input force signal,

978-1-4244-4524-0/09/$25.00 ©2009 AACC

which can rapidly excite the dynamic behavior of materials over a broadband. Second, the recently-developed model-less inversion-based iterative control (MIIC) technique [1] is utilized to eliminate the hardware adverse effects and allow precise application of such an excitation force to the material, as well as precise measurement of the consequent response of the material. The measured input-output data, i.e., the excitation force and the material response (indentation), are then used to obtain the frequency-dependent viscoelasticity of the material. The proposed NVBS is illustrated by implementing it to measure the viscoelasticity of a PDMS sample.

II. Feedforward Control Approach to Broadband Viscoelasticity Spectrum on SPM

A. Nanoscale Material Property Measurement using SPM

SPM is not only a unique tool to obtain nanoscale image of materials, but also becomes a powerful tool to characterize various nano-scale materials properties through the measurement of tip-sample interaction force, i.e., the force curve measurement [6]. To obtain the force curve, a micro-fabricated cantilever with a nano-size tip (see Fig. 1(a)) is driven under a piezoelectric actuator to push against the sample surface until the cantilever deflection (i.e., the tip-sample interaction force) reaches the setpoint value. Then the cantilever will retrace from the sample to a pre-determined distance. The force distance curve is obtained by measuring the tip-sample interaction force versus the vertical displacement of the SPM-tip during the push-retraction process (see Fig. 1(b)). The force curve contains the information of tip-sample interaction force and the indentation and thereby can be used to explore various material mechanical properties such as creep compliance, and Young's modulus [2].

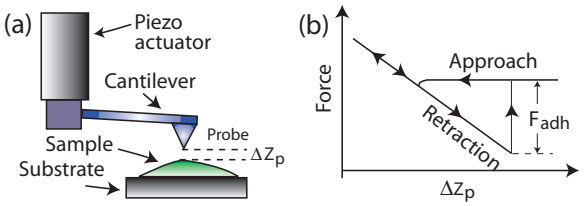

Fig. 1. The scheme of force curve measurement by SPM

B. Model-less Inversion-based Iterative Control

The MIIC control law, as schematically depicted in Fig. 2, can be described in frequency domain as follows:

$$u_0(j\omega) = \alpha z_d(j\omega), \qquad k=0,$$
$$u_k(j\omega) = \begin{cases} \frac{u_{k-1}(j\omega)}{z_{k-1}(j\omega)} z_d(j\omega), & \text{when } z_{k-1}(j\omega)\neq 0, \\ & \text{and } k\geq 1, \\ 0 & \text{otherwise} \end{cases} \quad (1)$$

where '$f(j\omega)$' denotes the Fourier transform of the signal '$f(t)$', '$z_d(\cdot)$' denotes the desired output trajectory, '$z_k(\cdot)$' denotes the output obtained by applying the input '$u_k(\cdot)$' to the system during the k^{th} iteration, and $\alpha \neq 0$ is a pre-chosen constant (e.g., α can be chosen as the estimated DC-Gain of the system).

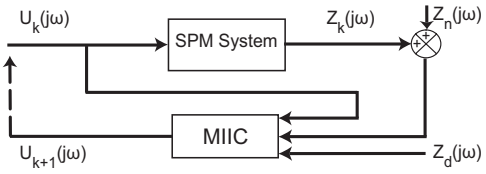

Fig. 2. The system diagram of the MIIC algorithm.

The convergence of the MIIC algorithm has been analyzed in [1]. We summarize the main results below.

Theorem 1: Let G($j\omega$) be a stable single-input-single-output (SISO), linear time invariant (LTI) system, and at each frequency ω, consider the system output z(t) to be affected by the disturbance and/or the measurement noise $z_n(t)$ as

$$z(j\omega) = z_l(j\omega) + z_n(j\omega), \quad (2)$$

where $z_l(j\omega)$ denotes the linear part of the system response to the input $u(j\omega)$, i.e. $z_l(j\omega) = G(j\omega)u(j\omega)$, and $z_n(j\omega)$ denotes the output component caused by the disturbances and/or the measurement noise. Then,

1) the ratio of the iterative input $u_k(j\omega)$ to the desired input $u_d(j\omega)$ is bounded in magnitude and phase, respectively, as

$$1-\varepsilon(\omega) \leq \lim_{k\to\infty} \left| \frac{u_k(j\omega)}{u_d(j\omega)} \right| \leq \frac{1-\varepsilon(\omega)}{1-2\varepsilon(\omega)}, \quad (3)$$

$$\lim_{k\to\infty} \left| \angle \left(\frac{u_k(j\omega)}{u_d(j\omega)} \right) \right| \leq \sin^{-1}\left(\frac{\varepsilon(\omega)}{1-\varepsilon(\omega)} \right), \quad (4)$$

provided that the noise to signal ratio (NSR) as defined below, is upper-bounded by a less-than-half constant, $\varepsilon(\omega)$,

$$\left| \frac{z_{k,n}(j\omega)}{z_d(j\omega)} \right| \leq \varepsilon(\omega) < 1/2, \quad \forall\ k, \quad (5)$$

where the desired input $u_d(j\omega)$ enables the linear part of the system output to exactly track the desired output, i.e., $z_d(j\omega) = G(j\omega)u_d(j\omega)$, and $z_{k,n}(j\omega)$ denotes the part of the output caused by disturbances and/or measurement noise in the k^{th} iteration.

C. Implementation of the MIIC Technique in NBVS

As conceptually depicted in Fig. 3, the use of the MIIC technique in the proposed NBVS is to "learn" and "cancel" the dynamics of the piezo-cantilever system for the given desired force signal $z_d(t)$, such that the output of the piezo-cantilever system, i.e., the force exerted onto the sample, $z_f(t)$, follows the desired force signal, $z_f(t) \to z_d(t)$. Thus the proposed approach is different from the multi-frequency excitation method [7] where the desired force-signal is applied to drive the piezo-cantilever system directly (see Fig. 3), resulting in the dynamics convolution of the piezo-cantilever system into the measured material response. The MIIC law can be ***computed*** offline (instead of online) directly in frequency domain—the time-domain iterative control input is obtained through the inverse Fourier transform, and then applied as a feedforward, open-loop control input to the system.

In the proposed NVBS, the MIIC technique is used to exert a band-limited white-noise type of input force to excite the

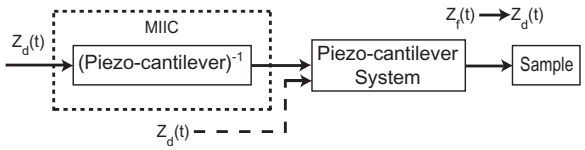

Fig. 3. The control input signal ($z_d(t)$) used by the NBVS and the multi-frequency excitation method to control the SPM system is input into the system at different enter points. The latter is represented with dash line.

nanomechanical behavior of soft materials, which is suitable for indentification of both nonparametric creep compliance function [2] and the parametric creep compliance model such as the truncated Prony series [8].

D. Identification of the Creep Compliance Model

We assume that the sample to be measured is a soft material. First, the MIIC technique is applied in force measurement of the soft material and a reference hard material to measure the indentation (i.e., the soft material's response). Second, the obtained input-output data are used in the Hertz contact mechanics model to obtain the complex compliance of the material in frequency domain. Finally, the creep compliance is modeled by a linear model (a truncated Prony series), and the parameters in the linear model is identified. We start with describing the indentation measurement.

1) Obtain the Excitation Force and the Indentation Response: In order to measure the response of the soft sample material to the excitation input (force), i.e., the indentation of the tip into the soft sample, the same control input (obtained from the use of the MIIC algorithm on the soft sample) is applied to measure the force curve on a reference hard material. The force applied from the tip to the sample during the force measurements can be obtained from the measured cantilever deflection signal by using the relation [2],

$$F_S = K_t \times C_t \times d_S, \tag{6}$$

where K_t is the stiffness constant of the cantilever, C_t is the sensitivity constant of the deflection signal vs. the vertical displacement of the tip (both can be experimentally calibrated [9]), and d_S denotes the cantilever deflection on the soft sample. Then, the indentation of the tip into the soft sample can be obtained as [6]

$$Z_I = C_t \times (d_H - d_S), \tag{7}$$

where d_H denotes the deflection on the hard material to the same control input for which the deflection on the soft material, d_S, is measured.

2) Obtain the Complex Compliance of the Material: Next, Hertz contact mechanics model [2] is utilized to extract the viscoelasticity of the material from the experimentally measured force and indentation data.

$$J(j\omega) = \frac{\left[h^{\frac{3}{2}}(\cdot)\right](j\omega)}{\mathscr{C}_1 \times P(j\omega)} \times \frac{1}{j\omega}, \tag{8}$$

where P(t) is the interaction force between the tip and the sample surface, h(t) is the indentation of the tip on the sample surface, J(t) is the creep compliance of the sample material in uniaxial compression, and the constant $\mathscr{C}_1$ is given by

$$\mathscr{C}_1 = \frac{3(1-\nu^2)}{4\sqrt{R}}, \tag{9}$$

where ν is the poisson ratio of the soft sample, and R is the tip radius.

Note that as commonly occurring in frequency response measurements, noise-like spikes might appear in the raw data plot of the complex compliance. Such noise-like spikes can be removed/filtered by using commercially available signal processing algorithms (such as the command '`spafdr`' in MATLAB). Second, we also note that the residual SPM-dynamics effect might still appear in the complex compliance at some frequencies, for example, around the resonant peaks—due to the sensitive variation of the SPM-dynamics around those frequencies, resulting in significant measurement errors in the creep compliance function. Thus, we introduce the parameterized-based approach to identify the creep compliance function.

3) Identification of the Creep Compliance Function Based on a Linear Prony Series Model: A linear creep compliance model is utilized to identify the time-domain creep compliance function. The use of the creep compliance model allows a substantial removal of the residual SPM dynamics effect from the measured data, and thereby obtaining a more accurate creep compliance function J(t). In this article, we use a truncated Prony series (i.e., a series of discrete exponential terms) to model the creep compliance [8].

$$J(t) = \left[J_0 + \sum_{i=1}^{n} J_i \cdot e^{-t/\tau_i}\right] \cdot 1(t), \tag{10}$$

where J_0 is the fully relaxed compliance, J_is are the compliance coefficients, τ_is are the discrete retardation times, and 1(t) is a unit step function

The corresponding complex compliance model J(jω), can be obtained from the Fourier transform of Eq. (10) as

$$J(j\omega) = \frac{J_0}{j\omega} + \sum_{i=1}^{n} \frac{J_i}{j\omega + 1/\tau_i}, \tag{11}$$

which can be further rewritten as the summation of the real part and the imaginary part.

$$J(j\omega) = \left(\sum_{i=1}^{n} \frac{J_i \cdot \tau_i \cdot \omega}{1+\tau_i^2 \cdot \omega^2}\right)\frac{1}{\omega} + \left[J_0 + \sum_{i=1}^{n} \frac{J_i \cdot \tau_i^2 \cdot \omega^2}{1+\tau_i^2 \cdot \omega^2}\right]\frac{-1}{\omega} j. \tag{12}$$

The parameters in the creep compliance model, $J_i s$ and $\tau_i s$, are identified via curve-fitting the experimentally measured storage and loss compliance (i.e., the real and the imaginary part in Eq. (8), respectively) with respect to the counterparts in Eq. (12), respectively.

Particularly, to reduce the numerical error in the fitting, we, priori to the fitting, remove the frequency scale effect of the '$j\omega$' term by multiplying '$j\omega$' on both sides of the Eq. (8) (when using it to plot the experimental data) and the model Eq. (12) (In the following, we call '$j\omega \cdot J(j\omega)$' the *frequency-scaled complex compliance*). Also note that the compliance coefficient $J_i s$ and the retardation constants $\tau_i s$ for i=1, $\cdots$, 4 appear in the fitting of both the real part and the imaginary part. Thus the average value of the fitting results is used for these parameters. Once the parameters of the linear creep compliance model are identified, the creep compliance function can be plotted according to Eq. (10).

III. Experimental Example: Frequency-dependent Viscoelastic Measurement of PDMS

The implementation of the proposed method is similar as in [6] and is omitted due to the space limit.

A. Experimental Results & Discussion

1) Tracking of the Band-limited White-noise Trajectory: First, the MIIC algorithm was applied to enable exerting, from the cantilever, a band-limited white-noise type of excitation force to the PDMS sample (Readers are referred to Ref. [6] for the preparation of the PDMS sample). A band-limited white-noise with a cut-off frequency of 4.5 KHz was generated in MATLAB for a time period of 6 seconds. Note that the bandwidth of the z-axis SPM dynamics (measured by 3dB drop of the gain) was at 1.27 kHz. Then the generated force trajectory was used as the desired trajectory in the MIIC algorithm and applied in the force measurement on the PDMS sample along with a small normal force. The small normal load was used to avoid the pull-off of the tip from the sample surface during the measurements. The iteration was converged in 3-5 iterations, and the converged output along with the desired trajectories and the tracking error are shown in Fig. 4. In addition, the tracking performance was also quantified in terms of the relative RMS error $E_2(\%)$ and the relative maximum error $E_\infty(\%)$, as shown in Table I.

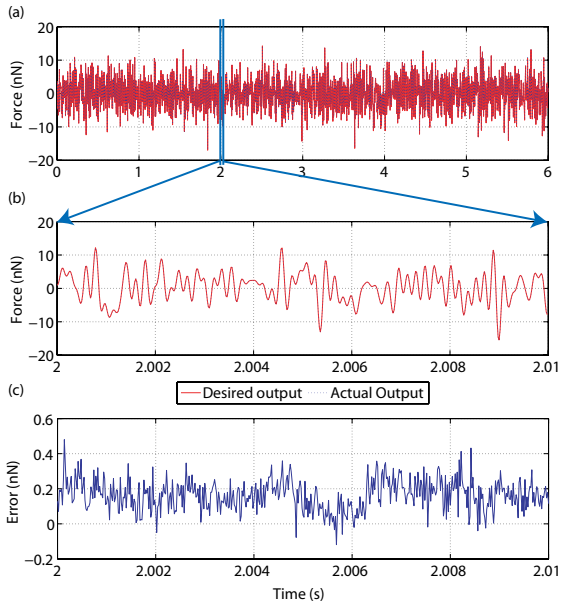

Fig. 4. (a) The experimental tracking result (i.e., the force applied to the PDMS sample, which was converted from the cantilever deflection) of the band-limited white-noise trajectory with a period of 6 sec., (b) the zoomed-in view of the tracking result for time t ∈ [2, 2.01] sec., and (c) the tracking error within the zoomed-in time window.

The experimental results show that by using the MIIC technique, precise output tracking of complex desired trajectories can be achieved. For the cut-off frequency of 4.5 kHz, the output tracking trajectory converged to the desired trajectories within 4 iterations. The precise exertion of such a complex excitation input force in the force measurement was difficult to achieve by using feedback control—if not entirely impossible, because the band-limit of the trajectory at 4.5 kHz was significantly higher than the bandwidth of the z-axis dynamics at 1.27 kHz, as shown in Fig. 5.

TABLE I
TRACKING PERFORMANCE OF THE MIIC TECHNIQUE.

Iter.No.	1	2	3	4	5
E_∞ (%)	44.05	15.85	6.09	6.13	4.31
E_2 (%)	7.14	4.52	5.12	5.25	4.69

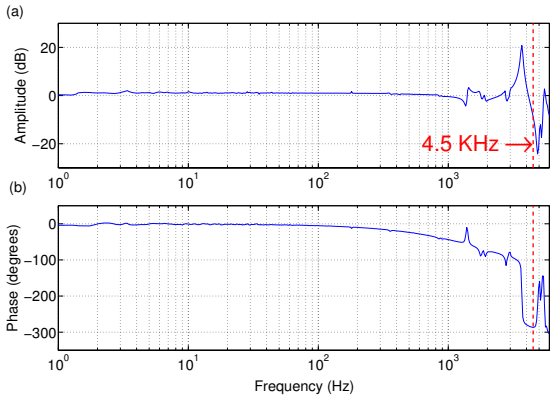

Fig. 5. The experimentally measured frequency response of the SPM dynamics in the z-axis direction.

The tracking precision of such complex trajectories can also be evaluated by comparing the power spectrum of the tracking result with the desired one in the frequency-domain. As can be seen from Fig. 6, the desired trajectory has rich frequency components across the entire frequency spectrum (Fig. 6 (a)), and the error of the power spectrum was maintained very small with no conspicuous difference at all frequency components (Fig. 6 (b)). Therefore, the experimental results show that the MIIC technique can be used to track complex force trajectory in force curve measurements.

2) The Force and the Indentation Measurements: The force applied on the PDMS sample was computed by Eq. (6), where the sensitivity constant of the cantilever of 85 nm/V was experimentally measured by following the method outlined in [9], and the cantilever spring constant of 0.065 N/m was calibrated by using the thermal noise method [9]. To measure the indentation, the converged iterative control input (obtained in Sec. 3.1.1 on the PDMS sample) was applied in the force measurement on the hard sapphire reference sample. The indentation of the SPM-tip into the PDMS sample was then calculated from the difference between the cantilever deflection on the PDMS sample and that on the sapphire sample (see Eq. (7)). The comparison of these two output deflection signals after the normal load being removed and the obtained indentation are shown in Fig. 7. We also plot the frequency components (the magnitude part) in the applied force and those in the corresponding indentation, i.e., the input and the output data in the identification experiment, in Fig. 8(a) and (b), respectively.

The experimentally measured force-indentation data reveal the frequency-dependent viscoelastic characteristics of the PDMS material. We note that compared to PDMS, sapphire sample can be practically regarded as "infinitely hard". Therefore, under the same control input to the z-axis piezo

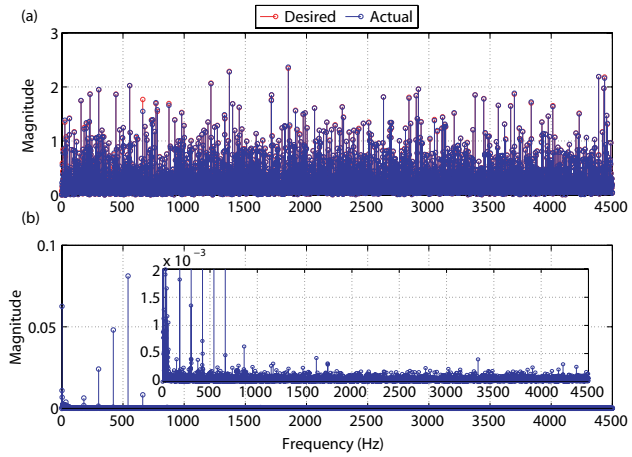

Fig. 6. (a) Comparison of the power-spectrum of the desired white-noise trajectory with the tracking result, and (b) the power spectrum of the error signal.

actuator (i.e., the same excitation force), the cantilever deflection obtained on the sapphire sample should be always larger than that on the PDMS sample. Such a prediction agreed with our experimental results: the indentation obtained in the experiments was always greater than zero (see Fig. 7 (c)). Furthermore, the experimental results also show that the indentation response of the PDMS sample was *frequency dependent*. As shown in Fig. 8 (b), the amplitude of the frequency components in the corresponding indentation presented a trend towards becoming smaller as frequency increased—except two spikes at around 1.4 kHz and 2.9 kHz. Such a trend also agreed with the rate-dependent viscoelastic properties of PDMS: as the excitation frequency increased, the movements of the molecules of the PDMS sample were significantly retarded since they cannot follow the external deformation fast enough, hence, a faster external deformation rate transitioned the viscoelastic response of PDMS from being rubbery toward being glassy. We note that the spikes in the indentation frequency plot (Fig. 8(b)) occurred around the frequencies where the z-axis SPM dynamics has resonant peaks (see Fig. 5), thus such spikes might be due to the residual SPM dynamics effect on the measured result. However, the trend of the rate-dependence of the indentation response was still pronounced in the experiments. Therefore, the experiment results demonstrate that the proposed NVBS technique can be used to measure frequency-dependent viscoelastic properties of materials over a large frequency range.

3) Complex Compliance Identification: By using the excitation force and the indentation data obtained from the experiments, the complex compliance J(jω) of the PDMS sample , as plotted in Fig. 9, can be calculated according to Eq. (8), where the probe radius of 57 nm was experimentally characterized by imaging a standard probe calibration sample (porous aluminum PA01) [9]. The improved complex compliance obtained by removing the "spikes" was used to identify the parameters. Particularly, a fourth-order Prony series model was used (n=4 in Eq. (12)), and the real part and the imaginary part of the frequency-scaled complex

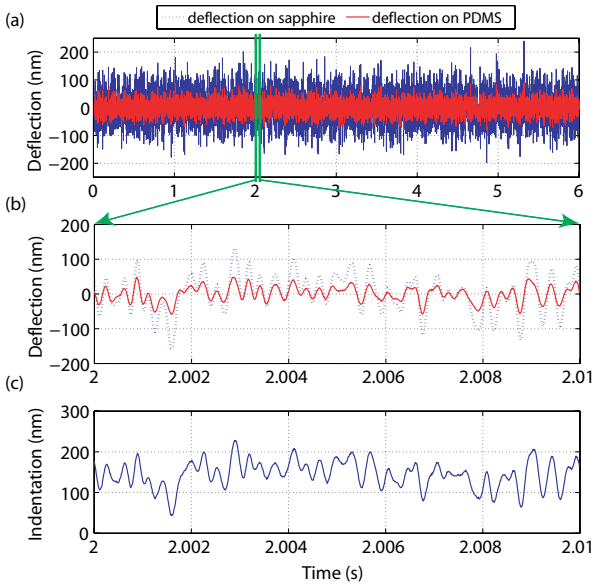

Fig. 7. (a) The comparison of the experimentally measured deflection signals on PDMS and that on a sapphire sample, (b) the zoomed-in view of plot (a) for time t $\in$ [2, 2.01] sec., and (c) the difference between these two deflection signals within the zoomed-in time window.

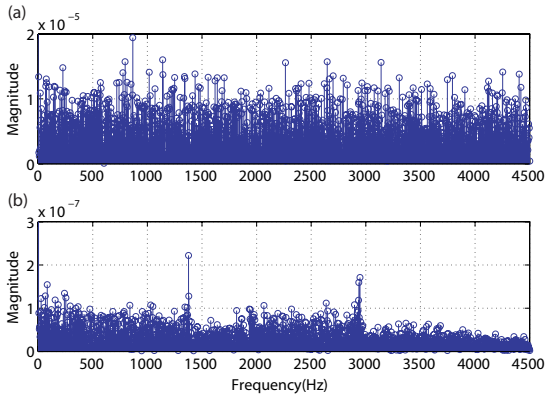

Fig. 8. (a) The tip-sample interaction force that shows the band-limited white-noise characteristic, and (b) the indentation into PDMS sample obtained under the force of (a).

compliance, $j\omega J(j\omega)$, were fitted separately by using the MATLAB command 'nlinfit' (see Eq. (12)), and the averaged values from these two fittings (the real-part and the imaginary part) were used for the parameters in the linear viscoelasticity model Eq. (12). The fitting results are compared with the averaged values in Table II, and also in Fig. 10 along with the experimental data. The fitting was quite well as the fitting errors were small. Table II also shows that the four fitted relaxation time constants occupied four different time orders, spanning from 0.01 ms to 0.01 s. The averaged parameters were used in the linear viscoelasticity model to plot the real-part and imaginary-part of the complex compliance, and compared to those of the experimental data, as shown in Fig. 10 with logarithmic-scale in frequency. After all the parameters J_i and τ_i in the 4^{th}-order Prony series model were estimated, the creep compliance in time domain was calculated from Eq. (10), and is shown in Fig. 11.

4) Discussion: According to calculated creep compliance, the instantaneous modulus of PDMS is about 1.33 MPa and it

TABLE II

THE PARAMETERS GENERATED FROM THE CURVE FITTING OF THE REAL PART AND IMAGINARY PART OF THE COMPLEX COMPLIANCE, AND THEIR AVERAGE.

Param.	Real Part	Imag. Part	Average
J_0 (Pa^{-1})	9.11×10^{-6}	NA	9.11×10^{-6}
J_1 (Pa^{-1})	-3.06×10^{-6}	-1.68×10^{-6}	-2.37×10^{-6}
J_2 (Pa^{-1})	-1.60×10^{-6}	-1.42×10^{-6}	-1.51×10^{-6}
J_3 (Pa^{-1})	-1.53×10^{-6}	-1.54×10^{-6}	-1.53×10^{-6}
J_4 (Pa^{-1})	-2.25×10^{-6}	-1.91×10^{-6}	-2.08×10^{-6}
τ_1 (sec.)	3.55×10^{-5}	6.61×10^{-5}	5.08×10^{-5}
τ_2 (sec.)	4.73×10^{-4}	4.57×10^{-4}	4.65×10^{-4}
τ_3 (sec.)	3.13×10^{-3}	2.67×10^{-3}	2.90×10^{-3}
τ_4 (sec.)	2.43×10^{-2}	2.63×10^{-2}	2.53×10^{-2}

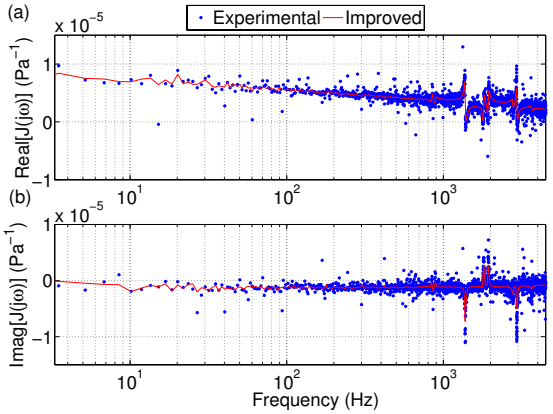

Fig. 9. The approximation of (a) the real part, (b) the imaginary part of the experimentally measured compliance of PDMS sample.

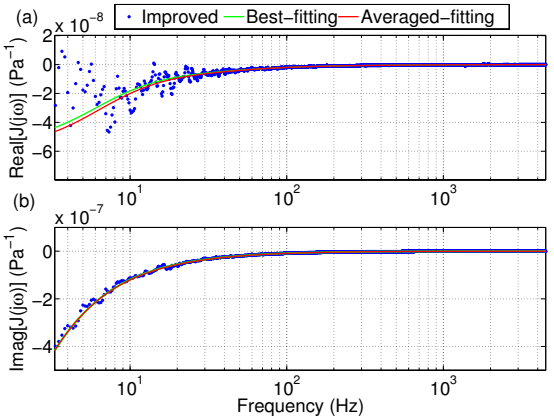

Fig. 10. The curve fitting results for (a) the real part, (b) the imaginary part of the experimentally measured compliance of the PDMS sample (i.e., without the frequency scale factor, $j\omega$).

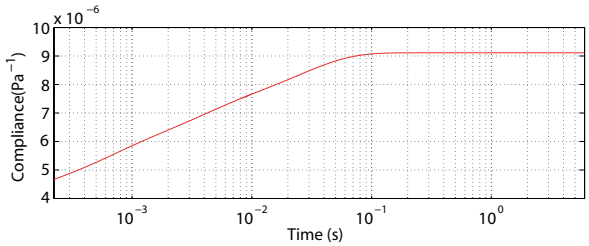

Fig. 11. The calculated compliance of PDMS sample in time domain by using the parameters obtained from the curve fitting with Eq. (10).

quickly relaxes to 0.2 MPa. The instantaneous and the static modulus were computed by setting time $t \to 0$ and $t \to \infty$ in the creep compliance model Eq. (10), respectively, and taking the inverse. Magnitude of the instantaneous and the fully relaxed modulus compare well with DMA tests on the same samples [6]. At room temperature, PDMS is above its glass temperature and displays a clear viscoelastic solid response. Our proposed characterization technique clearly captures the rate dependent viscoelastic nature of PDMS polymer. These results demonstrate the efficacy of our technique for rapid broadband viscoelastic characterization.

IV. CONCLUSION

In this paper, a novel nanoscale broadband viscoelasticity spectroscopy was proposed. In the proposed NBVS approach, the recently developed MIIC technique is used to I) the exertion of excitation force with broad frequency components onto the sample, and II) the measurement of the material response for such excitation (i.e., the material indentation). The frequency-dependent viscoelasticity of the material was then obtained by using the measured excitation force and the indentation in a contact mechanics model that describes the dynamics interaction between the probe and the sample. The proposed NVBS was illustrated by implementing it to measure the viscoelasticity of a PDMS sample.

REFERENCES

[1] K.-S. Kim and Q. Zou, "Model-less inversion-based iterative control for output tracking: Piezo actuator example," in *Proceedings of American Control Conference*, (Seattle, WA), pp. 2710–2715, June 2008.

[2] H.-J. Butt, B. Cappella, and M. Kappl, "Force measurements with the atomic force microscope: Technique, interpretation and applications," *Surface Science Reports*, vol. 59, pp. 1–152, 2005.

[3] E. Lupton, C. Nonnenberg, I. Frank, F. Achenbach, J. Weis, and C. Bräuchle, "Stretching siloxanes: An ab initio molecular dynamics study," *Chemical Physics*, vol. 414, pp. 132–137, 2005.

[4] A. S. A. Syed, K. J. Wahl, R. J. Colton, and O. L. Warren, "Quantitative imaging of nanoscale mechanical properties using hybrid nanoindentation and force modulation," *Journal of Applied Physics*, vol. 90, no. 3, pp. 1192–1200, 2001.

[5] K. Kim, Q. Zou, and C. Su, "A new approach to scan trajectory design and track: Afm force measurement example," *Journal of Dynamic Systems, Measurement and Control*, vol. 130, pp. 1–10, Sep. 2008.

[6] K. Kim, Z. Lin, P. Shriotrya, S. Sundararajan, and Q. Zou, "Iterative control approach to high-speed force-distance curve measurement using AFM: Time dependent response of PDMS example," *Ultramicroscopy*, vol. 108, pp. 911–920, Aug. 2008.

[7] J. R. Lozano and R. Garcia, "Theory of multifrequency atomic force microscopy," *Physical Review Letters*, vol. 100, pp. 1–4, Feb. 2008.

[8] M. L. Oyen, "Spherical indentation creep following ramp loading," *Journal of Materials Research*, vol. 20, p. 2094, Aug. 2005.

[9] J. L. Hutter and B. J., "Calibration of atomic-force miscroscope tips," *Review of Scientific Instruments*, vol. 64, no. 7, pp. 1868–1873, 1993.